Available online at www.sciencedirect.com

ScienceDirect

Advances in Space Research 54 (2014) 2131–2139

ADVANCES IN SPACE RESEARCH (a COSPAR publication)

www.elsevier.com/locate/asr

Influence of lunar topography on simulated surface temperature

Meng Zhiguo [a,b,c,*], Xu Yi [b], Cai Zhanchuan [b], Chen Shengbo [a], Lian Yi [a], Huang Hang [a]

[a] *College of Geoexploration Science and Technology, Jilin University, Changchun 130026, China*
[b] *Space Exploration Laboratory, Macau University of Science and Technology, Macau, China*
[c] *Key Laboratory of Lunar and Planetary Exploration, National Astronomical Observatories, CAS, Beijing 100012, China*

Received 3 December 2012; received in revised form 15 May 2014; accepted 17 May 2014
Available online 2 June 2014

Abstract

The surface temperature of the Moon is one of the essential parameters for the lunar exploration, especially to evaluate the Moon thermophysical features. The distribution of the temperature is heavily influenced by the Moon topography, which, however, is rarely studied in the state-of-art surface temperature models. Therefore, this paper takes the Moon topography into account to improve the surface temperature model, Racca model. The main parameters, such as slopes along the longitude and latitude directions, are estimated with the topography data from Chang'E-1 satellite and the Horn algorithm. Then the effective solar illumination model is then constructed with the slopes and the relative position to the subsolar point. Finally, the temperature distribution over the Moon surface is obtained with the effective illumination model and the improved Racca model. The results indicate that the distribution of the temperature is very sensitive to the fluctuation of the Moon surface. The change of the surface temperature is up to 150 K in some places compared to the result without considering the topography. In addition, the variation of the surface temperature increases with the distance from the subsolar point and the elevation, along both latitude and longitude directions. Furthermore, the simulated surface temperature coincides well with the brightness temperature in 37 GHz observed by the microwave sounder onboard Chang'E-2 satellite. The corresponded emissivity map not only eliminates the influence of the topography, but also hints the inherent properties of the lunar regolith just below the surface. Last but not the least, the distribution of the permanently shadowed regions (PSRs) in the lunar pole area is also evaluated with the simulated surface temperature result.

Keywords: Surface temperature; Moon topography; Improved Racca model; LAM data; Effective solar illumination

1. Introduction

The surface temperature distribution is one of the fundamental thermophysical parameters for the Moon research, and essential to interpret the thermal emission information from the regolith, especially to analyze the data collected by microwave sounder (Chen et al. 2010; Jiang et al., 2008). The microwave sounders onboard Chang'E satellites have measured the global brightness temperature of the Moon (Wang et al., 2010). The application of such data, however, encounters critical problems, one of which resides in estimating the surface temperature (Krotikov and Troitsky, 1964; Keihm and Langseth, 1975; Schloerb et al., 1976; Naugol'naya and Soboleva, 2001; Jiang et al., 2008; Li et al., 2008). The surface temperature of Moon varies considerably with the relative position of the measured point to the subsolar point. Unlike geologically active bodies, the Moon no longer has an internal heat source, thus the heating comes almost entirely from the Sun (Jones et al., 1975; Heiken et al., 1991). Therefore, precise estimation of the surface temperature will greatly benefit the thermal research, e.g. thermal evolution of the

* Corresponding author. Permanent address: No. 938 Ximinzhu Street, Changchun 130026, China. Tel.: +86 431 88502362.
E-mail address: mengzg@jlu.edu.cn (M. Zhiguo).

http://dx.doi.org/10.1016/j.asr.2014.05.015
0273-1177/

Moon, and the selection of the lunar landing sites (Neal, 2009).

Currently, there are several methods to obtain the lunar surface temperature, including the direct measurement during the Apollo missions, the estimation from the earth-based observation and the simulation with theoretical models (Racca, 1995; Li et al., 2007). The last approach is widely used in Moon research due to its high accuracy contributed by the various input parameters, such as solar illumination, dielectric constants, emissivity, albedo and internal thermal flux of the lunar regolith. Wesselink (1948) constructed a surface temperature model to interpret the thermophysical parameters of the lunar material, assuming that the surface temperature is changing either in associated cosine function or in Fourier series. Viewing the Moon surface material as gray body, Jaeger (1953) established the temperature model by considering the temporal change of the solar illumination. Jones et al. (1975) simulated the Moon surface temperature with thermal conductivity equation, which considered not only the changes of the solar illumination but also the ellipse parameters to obtain the surface temperature during lunar eclipse. Li et al. (2008) simulated the surface temperature using thermal conduction equation and the thermophysical parameters obtained from Moon samples. According to the conservation of energy and the thermal conduction equation, Racca (1995) deduced the relation between the surface temperature and the solar illumination, thermal emission, absorption and the internal thermal flux in steady state and transient behavior. Compared with aforementioned models, the model constructed by Racca, named as Racca model in this paper, is derived with energy conservation and thermal conduction in the lunar regolith and takes the internal thermal flux into account. Moreover, the surface temperature in steady state is of great interest to scientists. Therefore, the Racca model for steady state is adopted and improved in this study.

As an important influential factor, the solar illumination is employed in all Moon surface temperature models, including Racca model (Racca, 1995; Li et al., 2007). However, previous surface temperature research focused on the influence of the effective solar illumination and the relative position of the measured point to the subsolar point on the final surface temperature and ignored the impact of topography on the solar illumination (Jaeger, 1953; Jones et al., 1975; Racca, 1995; Li et al., 2009). The great hills and the huge craters are widely spread on the Moon surface (Heiken et al., 1991), and such fluctuation of the terrain may heavily affect the distribution of the effective solar illumination. Bussey et al. (2009) introduced a model to determine the illumination and thermal conditions inside the permanently shadowed regions near the lunar pole regions. The result shows that the thermal condition within the crater is highly affected by its terrain. To study the ice deposit in pole regions, Vasavada et al. (1999) took the terrain into consideration and simulated the temperature distribution in bowl-shaped and flat-floored craters. Based on Diviner data, Paige et al. (2010) presented the surface-temperature maps, which also demonstrated that the temperature distribution is heavily influenced by the topography. Bussey et al. (2010) and Mazarico et al. (2011) studied the permanently shadowed regions in both poles of the Moon using Kaguya topography and LOLA (Lunar Orbiter Laser Altimeter) topography, respectively. However, the influence of the topography on the surface temperature is still uncovered.

Therefore, to simulate the surface temperature, the influence of the topography should be considered and quantified. In this paper, to study the influence of the topography on the surface temperature, the Laser Altimeter (LAM) data from Chang'E-1 satellite and the Horn algorithm are used to produce the topographic features of the Moon. Section 2 introduces the improved Racca model according to the surface topography; Section 3 presents the LAM data and methodology used to produce the topographic features of the Moon; Section 4 provides the results of the simulated lunar surface temperature considering both solar illumination and topography; Section 5 is the conclusion and discussion.

2. Improved temperature model

According to the thermal conduction theory of the semi-finite material, the lunar surface temperature is affected by two thermal sources: the solar radiation and the internal thermal flux of the Moon (Jones et al., 1975). Based on the Stefan–Boltzmann rule, the relation between the temperature and the thermophysical parameters can be constructed by solving the thermal conduction model (Jones et al., 1975; Racca, 1995).

2.1. Lunar surface temperature model

Considering a lunar unit surface at latitude ϕ_1 and longitude φ_1, the steady state surface temperature T_0 can be expressed as (Racca, 1995):

$$T_0(\phi_1, \varphi_1) = \left[\frac{1-\alpha}{\varepsilon}\frac{S}{\sigma} + \frac{Q}{\sigma}\right]^{1/4} \tag{1}$$

where ε is the thermal emissivity of the regolith. α is the albedo. Q is the inner thermal flux. $\sigma = 5.67 \times 10^{-8}$ W rn^{-2} K^{-4} is the Stefan–Boltzmann constant and S is the effective solar radiation.

Given the slope of the surface is 0 (Fig. 1), S in the measured position (ϕ_1, φ_1) can be expressed as

$$S = S_0 \cos{}' \cos \varphi' \tag{2}$$

where S_0 is the total solar illumination, (ϕ_0, φ_0) is the subsolar point of the Sun light, and $\phi' = |\phi_1 - \phi_0|$ and $\varphi' = |\varphi_1 - \varphi_0|$ are the corresponding solar angles of the measured unit along the longitude and latitude, respectively.

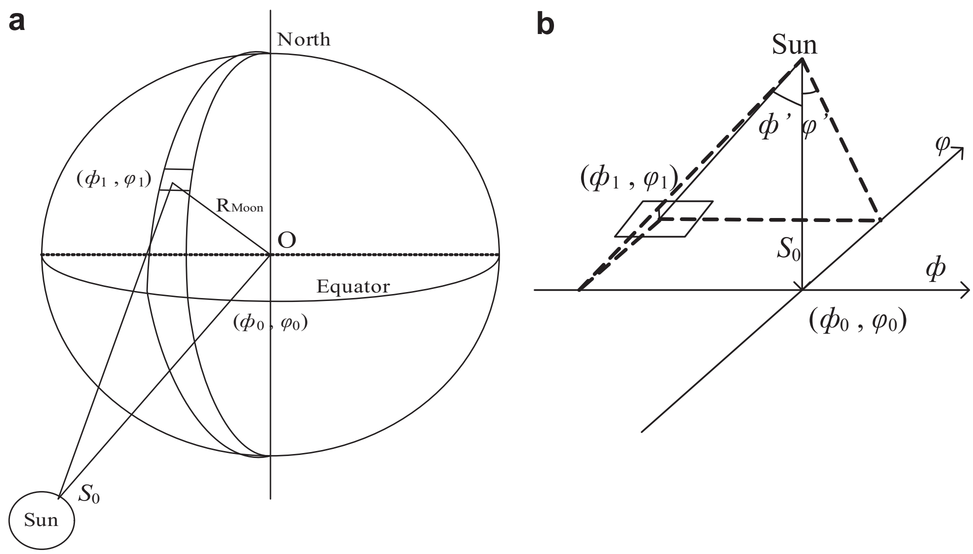

Fig. 1. Schematic diagram of solar radiation incidence angle on the lunar surface O is the geometric center of the Moon. (ϕ_0, φ_0) is the subsolar point of the Sun light. (ϕ_1, φ_1) is the measured point.

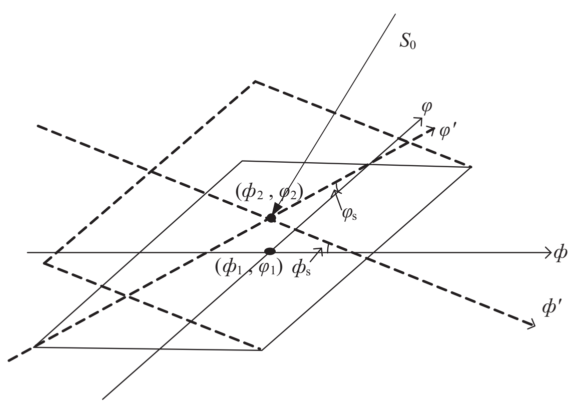

Fig. 2. Topography influence on the effective solar radiation.

Therefore, if the real surface is inclined and the slope is ϕ_s in longitude direction and φ_s in latitude (Fig. 2), the theoretical effective solar illumination is

$$S = S_0 \cos('-{}_s)\cos(\varphi' - \varphi_S) \tag{3}$$

However, the actual topography is fairly complicated and the slope of the surface may be positive or negative relative to the direction of solar radiation. In a region where the surface slope is negative and the absolute value of the slope is large enough, which makes $(\phi' - \phi_s) > 90°$ or $(\varphi' - \varphi_s) > 90°$, the region will be in the shadow with no solar radiation. Therefore, the Racca's surface temperature model can be improved as

$$T_0(\phi', \varphi') = \left[\frac{1-\alpha}{\varepsilon}\frac{S}{\sigma} + \frac{Q}{\sigma}\right]^{1/4} = \begin{cases} \left[\frac{1-\alpha}{\varepsilon}\frac{S_0\cos(\phi'-\phi_s)\cos(\varphi'-\varphi_s)}{\sigma} + \frac{Q}{\sigma}\right]^{1/4}, & \phi' - \phi_s \leqslant 90°, \varphi' - \varphi_s \leqslant 90° \\ \left(\frac{Q}{\sigma}\right)^{1/4}, & other \end{cases} \tag{4}$$

2.2. Improved surface temperature model

Eq. (1)shows that the effective solar radiation is one of the essential factors to estimate the lunar surface temperature. However, in the previous studies, the influence of the topography is rarely considered in the simulation of the lunar surface temperature. The results by Li et al. (2008), Bussey et al. (2010) and Mazarico et al. (2011) demonstrate that the effective solar radiation is strongly affected by the topography, which will inevitably influence the surface temperature.

Eq. (4) tells that if the position of the measured point relative to the subsolar point as well as its slope is known, the influence of the topography on the actual surface temperature can be evaluated.

3. Data and methodology

Kaguya Topography data and LOLA topography data have been employed by Bussey et al. (2010) and Mazarico et al. (2011), respectively, to estimate the illumination conditions of the Moon surface. Onboard Chang'E-1 satellite, Laser Altimeter (LAM) has collected elevation data overlapping the whole Moon surface with higher accuracy (Ping et al., 2009). Thus, the LAM data and the Horn algorithm (Zhou and Liu, 2006) are employed to evaluate the influence of the Moon topography on the surface temperature.

3.1. LAM data

The Chang'E-1 satellite is the first Chinese lunar orbiter. The laser altimeter, one of the key payloads of Chang'E-1 (CE-1), is used to measure the altitude of the entire Moon surface, and the lunar topography can be obtained with these range measurements (Ping et al., 2009; Li et al., 2010).

Till Dec. 4th, 2008, LAM has obtained 9.12 million original altimetry data over 1000 orbits that cover the entire lunar surface. More than 8 million range measurements from the Chang'E-1 Laser Altimeter have been used to produce a global topographic model of the Moon with improved accuracy (Ping et al., 2009; Li et al., 2010). CLTM-s01 (Chang'E Topographic Model), developed by Ping et al. (2009), is a 360th degree and order spherical harmonic expansion. The absolute vertical accuracy of CLTM-s01 is 31 m and the spatial resolution is 0.25° (~7.5 km) (Ping et al., 2009). Considered that the goal of our study is to evaluate the influence of the topography on the surface temperature, the CLTM-s01 elevation data (Fig. 3) is accurate enough for extracting the surface topography information.

3.2. LAM data processing

Slope is an important parameter to represent the fluctuation of the topography. Currently, the slope is always estimated by analyzing the digital elevation data (Tang et al., 2005; Zhou and Liu, 2006). Based on the grids used in calculation, the analyzing methods for calculating the surface slope can be categorized as Maximum Gradient Method, Second Finite Difference, Horn algorithm (Tang et al., 2005; Zhou and Liu, 2006). The Horn algorithm is

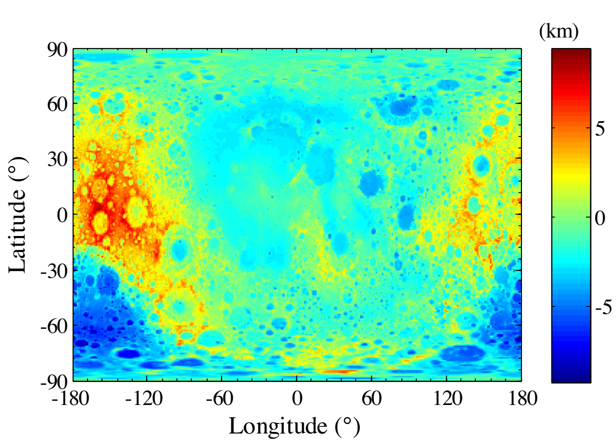

Fig. 3. Lunar surface altitude map.

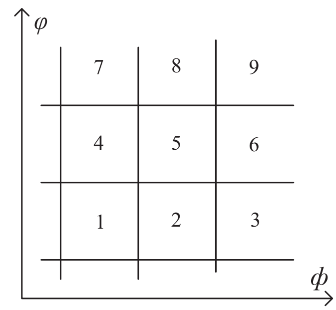

Fig. 4. 3 × 3 Local mobile window for LAM.

applicable to estimate the slope of any kind of topography (Chen et al., 2009), thus it is adopted in this study.

In the two-dimensional plane ϕ–φ composed by LAM data z_i (Fig. 4), the inclination rate of the terrain, f_ϕ along the longitude and f_φ along the latitude, can be calculated with the Horn algorithm using a 3 × 3 local mobile window as shown in Fig. 4.

$$\begin{aligned} f_\phi &= \frac{z_3 - z_1 + 2(z_6 - z_4) + z_9 - z_7}{8g} \\ f_\varphi &= \frac{z_7 - z_1 + 2(z_8 - z_2) + z_9 - z_3}{8g} \end{aligned} \tag{5}$$

where, $z_i (i = 1, 2, \dots, 9)$ is the LAM data, g is the distance between the center of the two adjacent pixels. The corresponding slopes along the longitude and the latitude can be expressed as

$$\phi_s = \arctan(f_\phi), \quad \varphi_s = \arctan(f_\varphi) \tag{6}$$

Therefore, the slopes at any position of the Moon can be obtained.

The above calculation is based on the assumption that the change of the topography is positive if the pixel values in the west are higher than those in the east or the pixel values in the north are higher than those in the south. Otherwise, the changes are negative. However, the illumination conditions over the Moon surface are complicated. Even the same slope may have different effects on the effective solar illumination. Assuming the pixel values in the west are larger than those in the east in the measured point, the slope should be positive. But if the measured point locates in the west relative to the subsolar point, the point will experience more effective illumination. Otherwise, the effective illumination will be less.

To solve the problem, the Moon surface is divided into four parts and the boundaries are the central longitude and central latitude of the subsolar point (Fig. 5). Then the effective solar illumination can be express as

$$S = \begin{cases} S_0 \cos(\phi' + \phi_s)\cos(\varphi' - \varphi_s), & \mathrm{I} \\ S_0 \cos(\phi' - \phi_s)\cos(\varphi' - \varphi_s), & \mathrm{II} \\ S_0 \cos(\phi' + \phi_s)\cos(\varphi' + \varphi_s), & \mathrm{III} \\ S_0 \cos(\phi' - \phi_s)\cos(\varphi' + \varphi_s), & \mathrm{IV} \\ 0, & \mathit{other} \end{cases} \tag{7}$$

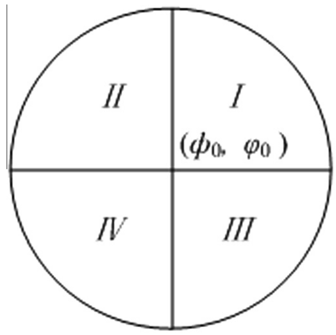

Fig. 5. Blocking model of the Moon surface.

where the condition for I, II, III and IV is $(\phi' - \phi_s) < 90°$ and $(\varphi' - \varphi_s) < 90°$. S is zero on condition that $(\phi' - \phi_s)$ or $(\varphi' - \varphi_s)$ is bigger than 90°.

With Eqs. (4) and (7), the lunar surface temperature influenced by the topography can be simulated.

4. Results and discussion

To simulate the lunar surface temperature, several essential surface thermophysical parameters should be studied thoroughly, including thermal emissivity ε, solar albedo α, and the total solar radiation S_0. According to the previous work (Logan et al., 1972; Smith and West, 1983; Neukum et al., 1991; Racca, 1995), $\varepsilon = 0.97$, $\alpha = 0.127$, $Q = 6\ \mathrm{W\ m^{-2}}$ and $S_0 = 1371\ \mathrm{W\ m^{-2}}$ are reasonable and adopted in this study. Then based on the LAM data and Eq. (4), the surface temperature at any time of the Moon can be obtained.

4.1. Surface temperature simulation

Assuming the subsolar point is (0°N/0°E), the surface temperature on the nearside of the Moon can be simulated (Fig. 6). Fig. 6 shows the simulated surface temperature, where the influence of the topography is not considered in Fig. 6(a) and that is considered in Fig. 6(b). Fig. 6 indicates that the topography strongly affects the distribution of the surface temperature, which results in the fluctuations of the temperature distribution. In general, the distribution of the temperature is apparently corresponding to the variation of the terrain, especially in the regions far from the subsolar point such as Mare Smythii (1 18′N/87°30′E) and Mare Orientale (19 24′S/92°48′W).

Furthermore, Fig. 6 also shows that the variation of the temperature are greater in the south and north polar regions. An interesting phenomenon is observed in Cabeus crater, located in 84°S to 85.6°S and 30°W to 45°W in south polar area. The simulated temperature in Cabeus crater is much lower than that in other places along the same latitude. This agrees well with the conclusion of Heiken et al. (1991) that Cabeus crater is a permanently shadowed region.

The comparison between Fig. 6(a) and (b) presents that the alternation of the temperature is regular. Around the subsolar point, the alternation of the temperature in near and middle areas is less than 40 K. The change increases with the distance from the subsolar point and with the variation of elevation, along both latitude and longitude directions. The most apparent changes occur in regions along the longitude 85°W and 85°E and in the polar areas. In some places such as Mare Smythii (1°18′N/87°30′E) and Mare Orientale (19°24′S/92°48′W), the difference of the simulated surface temperature is up to 150 K, which is almost the same as its flat surface temperature.

4.2. Relationship between surface temperature and topography

Fig. 7 is the simulated temperature along the longitude 0° and the latitude 0°, where Curve 1 and Curve 2 represent the temperature that considers the topography or not, respectively. Curve 3 is the relative elevation data. Fig. 7 shows that the influence of the topography on the surface temperature is strong. And the drastic changes of the temperature in Curve1 are always corresponding to the obvious fluctuations of the topography in Curve 3. If a place with positive slope locates in the west or in the north relative to subsolar point, it will receive more solar radiation

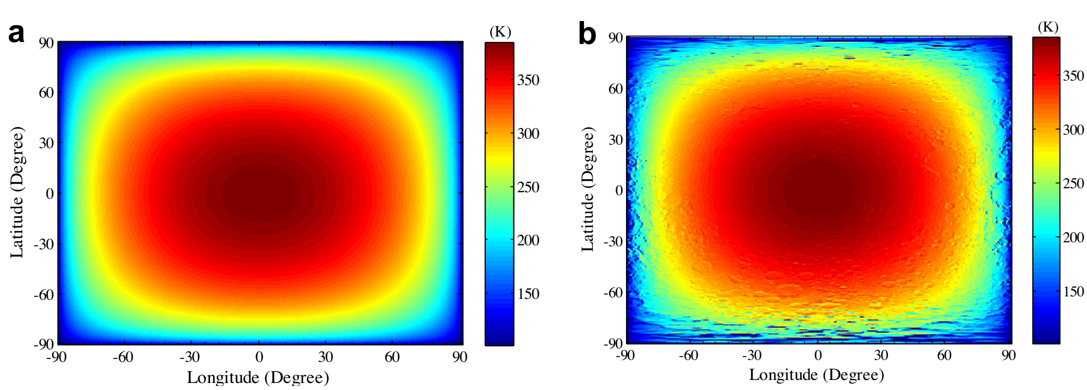

Fig. 6. Simulated lunar surface temperature. (a) Without considering topography. (b) Considering topography. The parameters used in the above simulation are $\alpha = 0.127$, $\varepsilon = 0.97$, $Q = 6$, $S_0 = 1371$.

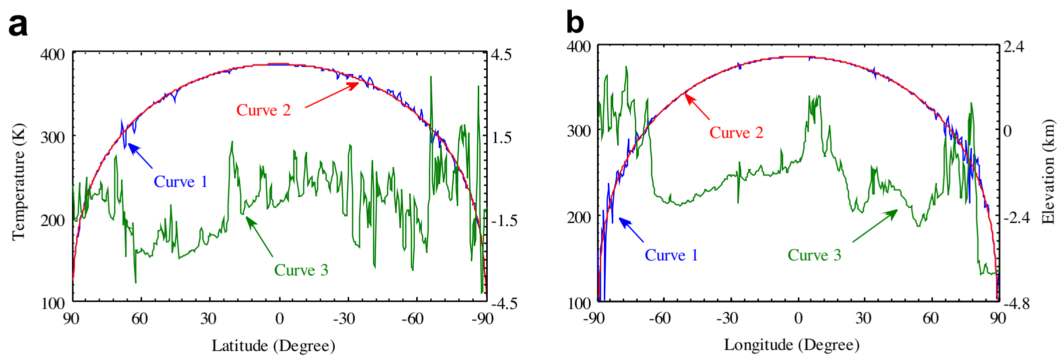

Fig. 7. Simulated temperature along the longitude 0° (a) and the latitude 0° (b). The influence of topography is considered in Curve 1 but it is not considered in Curve 2. Curve 3 is the relative elevation data along longitude 0° in (a) and latitude 0° in (b).

and therefore the temperature will become higher than the theoretical value in Curve 2. Otherwise, the surface temperature will decrease. As for a crater in north hemisphere, such as W. Bond crater at 65°18′N/0°E, the temperatures become lower along the south side of the crater but higher in the north side than those without considering the variation of elevation. The distribution of the simulated temperature in Curve 1 is apparently coincided with this observation.

The correlation analysis is conducted between the simulated temperature along latitude 0° and the elevation data. The correlation coefficient is only about 0.0148, which gives a weak correlation. In viewing that the influence from topography on the temperature is different in the east and west hemisphere, the same correlation is done for the data in the east hemisphere and the west hemisphere, respectively. The results show that the coefficients are 0.59 for the east part and 0.45 for the west, which inevitably posts that the influence of the topography on the surface temperature is directly correlated with its relative position on the Moon surface.

Meanwhile the correlations between the amount of the surface temperature change (which is the difference between Curve 1 and Curve 2 in Fig. 7) and the slope along latitude 0° and longitude 0° are also estimated. The correlation coefficient is about 0.68 along the latitude 0° while it is about 0.86 along the longitude 0°. It hints that the correlation between the surface temperature change and the alternation of the topography is much higher than previous results. Therefore, the influence from topography should not be neglected in the study of the surface temperature over the Moon surface.

4.3. Surface temperature versus microwave brightness temperature

To evaluate the simulated surface temperature, the microwave brightness temperatures in high frequencies are employed because the microwave at higher frequencies has the lower penetration depth, which makes brightness temperature be strongly influenced by the surface temperature and weakly affected by the uncertain regolith parameters such as the particle sizes and the surface roughness (Ulaby et al., 1981; Wang et al., 2010).

Onboard Chang'E-2 satellite, the four-channel microwave sounder (CELMS) operates at four frequency channels including 3, 7.8, 19.35 and 37 GHz to measure the brightness temperature of the Moon (Chen et al., 2010). Then the brightness temperature at 37 GHz channel (Fig. 8(b)) is employed to compared to the simulated surface temperature (Fig. 8(a)). Suppose the solar azimuth is 30°, and the solar elevation angle is only decided by its latitude for any measured point, the global surface temperature could be simulated in Fig. 8(a). And the brightness temperature with the same solar azimuth is also selected from observed CELMS data. Fig. 8 postulates that the distribution of the brightness temperature is apparently related to the surface temperature. They have nearly the same features along the longitude and latitude. The influence of the topography on the temperature distribution is obviously in high latitude regions, especially in the high latitudes such as Clavius crater (58.4°S/14.4°W), Cabeus crater (84.9°S/35.5°W) and Birkhoff crater (58.7°N/46.1°W).

However, the distributions of the simulated temperature and the observed brightness temperature do not coincide well with each other in low-latitude regions. The brightness temperature is much higher in Oceanus Procellarum and Mare Tranquillitatis than that along the same latitude. Considered that the penetration depth of the microwave used is about 10 cm at 37 GHz (Jiang et al., 2008; Li et al., 2010), it is inevitably the physical properties of the subsurface materials that result in the inconsistency, which in turn shows that it is feasible to extract the lunar regolith parameters with the CELMS data. To retrieve the lunar regolith parameters from the CELMS data, the influences from the topography on the surface temperature should be considered and removed at first.

In theory, if the change of the dielectric constants with temperature is neglected, the emissivity of the regolith will be fixed over the whole lunar day because the emissivity depends solely on the dielectric constants and the structure of the lunar regolith (Ulaby et al., 1981). We set the effective temperature of the regolith equal to the surface temperature as an approximation. Hence, the observed

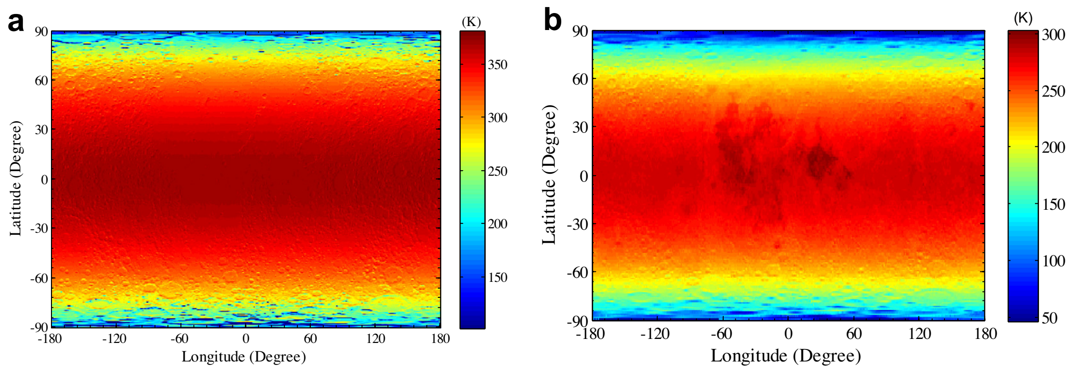

Fig. 8. Simulated lunar surface temperature (a) and observed brightness temperature (b). (a) is the global temperature with the assumption that the solar azimuth is 30°, and the solar elevation angle is only decided by its latitude for any measured place. (b) Microwave brightness temperature in 37 GHz observed by Chang'E-2 satellite with the solar azimuth 30°.

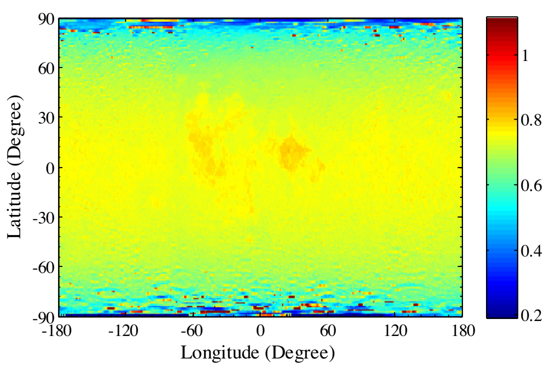

Fig. 9. Estimated emissivity map of the Moon at 37 GHz, solar azimuth is 30°.

brightness temperatures are divided by the simulated surface temperatures, the results of which can be seen as the emissivity of the lunar regolith (Fig. 9). Fig. 9 indicates that, apparently, the influence of the topography on the emissivity is eliminated. Fig. 9 also postulates that surface emissivity is largely ranging from 0.7 to 0.95 and it is higher in Mare than that in highlands. This coincides with the results by Meng et al. (2010) and Chen et al. (2010). That is, the simulation of the surface temperature is largely acceptable. However, there still exist abnormal regions in higher latitude regions, where the emissivity is much larger or smaller than that in other regions. And the research on surface temperature with other source data will provide further information about the nature of the regolith.

4.4. Abnormal temperature distribution in polar region

Research on permanently shadowed regions (PSRs) is one of the essential problems in the current Moon study. The PSRs are the places that never receive direct solar illuminations. That is to say, at any time of a day, the regions are in the shadow and the effective solar illumination of the regions is zero. Therefore, to any point over the Moon surface, we can simulate the temperature vector during a day (supposing the solar azimuth is changing from 0° to 180°) by improved Racca model and find out the highest temperature. If the highest temperature is much less than that in other places of the same latitude, it hints that the site is likely to be PSR.

Fig. 10(a) is the distribution of the highest temperature for any point in a day. It shows that there exist the obvious temperature abnormal regions in the south and north polar regions. The Cabeus crater in 84.9°S/35.5°W is known as a PSR, and the temperature here is much lower than that in the same latitude and with the same solar illumination. The

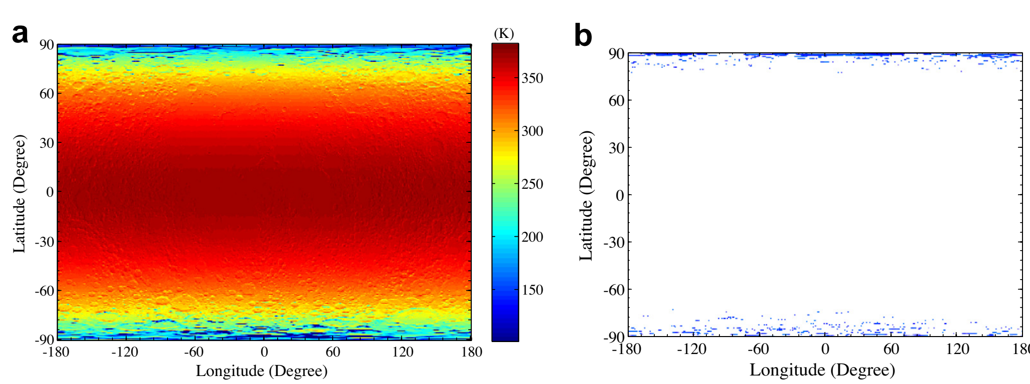

Fig. 10. Highest lunar surface temperature map (a) and abnormal temperature map (b). (a) is the global temperature on the condition that the solar azimuth is 0°, and the solar elevation angle is 0° for any measured place. (b) is the abnormal temperature map.

Table 1
Comparison of area in PSRs in the south and north polar areas.

	North (km^2)	South (km^2)
Meng et al.	11,274	6076
Mazarico et al. (2011)	12,866	16,055
Noda et al. (2008)	1236	4466
Bussey et al. (2003)	12,500	6500

regions of the same kind are widely distributed in the polar area.

Fig. 10(b) is the abnormal temperature map, where the blue point says that the highest temperatures in a day here are 101.4243 K, which is calculated with Eq. (1)when the effective solar illumination is zero. That is, the temperature here is only decided by the internal thermal flux in Eq. (1)and the map is also the distribution of the PSRs. Fig. 10 indicates that the PSRs are widely distributed in the both pole regions. In the north polar area, the PSRs are nearly all exist in the places where the latitude is higher than 85°N, while the lowest latitude in the south is up to the latitude 78°S. Moreover, the area of individual regions in north polar area is obviously larger than that in the south.

Statistical results show that the total area of the PSRs are about 11,274 km^2 in the north polar area and 6076 km^2 in the south (respectively 4.12% and 2.19% of the total region area). This is significantly lower than that estimated by Mazarico et al. (2011), while it is close to the result by Bussey et al. (2003) (Table 1). Table 1 postulates that the improved Racca model is also a possible way to study the PSRs in the Moon research.

We note that in Polar Regions, the surface temperature may experience more influential factors such as the weak solar illumination, the multi-reflection of the solar illumination, and so on. In addition, the collected brightness temperature data are affected by the spatial resolution of the microwave sounder, physical characteristics of the lunar regolith and the multi-reflection of the microwave thermal radiation at such regions. Thus, the abnormal emissivity values obtained by the proposed model may not be sufficient to identify PSRs, which requires further study.

5. Conclusions

This work focuses on studying the influence of topography on the Moon surface temperature. The surface temperature simulation model, Racca's model, is improved by incorporating the Moon topography as an influential factor. The LAM topography data obtained from Chang'E-1 satellite is employed to estimate the effective illumination with Horn algorithm and to study the influence of the topography on the surface temperature. The comparison between the surface temperature considering the topography and the temperature without considering the topography is conducted in this study. The results indicate that the surface temperature is heavily affected by the topography and the extent of the influence is different over the Moon surface. The fluctuation of the temperature becomes greater with the distance farther from the subsolar point and with the variation of elevation becoming greater. The comparison between the simulated surface temperature and the observed microwave brightness temperature in 37 GHz shows that the distribution of two temperature datasets is highly similar to each other. And the emissivity distribution estimated by the simulated temperature and the observed brightness temperature not only eliminates the influence of the topography, but also provides the inherent properties about the lunar regolith just below the surface, which indicates that the topography aware surface temperature model is reasonable and more accurate than the original Racca model. The improved temperature model can also be used for further study of the lunar regolith properties with other source data. The distributions of the permanently shadowed regions are also analyzed based on the simulation result.

Nevertheless, the total solar radiation and its seasonal and annual changes should also be taken into account in the surface temperature study. Meanwhile, the causes of the abnormal emissivity in pole regions deserve further study. These problems will be studied in our future work.

Acknowledgments

The LAM data are provided by National Astronomical Observatories, Chinese Academy of Sciences. The CELMS data are provided by Dr. Zheng Yongchun, researcher of National Astronomical Observatories, Chinese Academy of Sciences.

This work is supported by National Natural Science Foundation of China (Grants Nos. 41371332 and 40901159), China Postdoctoral Science Foundation (No. 2012M511341), and the Science and Technology Development Fund of Macau (No. 048/2012/A2).

References

Bussey, D.B., McGovern, J.A., Spudis, P.D., Neish, C.D., Noda, H., Ishihara, Y., Sorensen, S.A., 2010. Illumination conditions of the south pole of the Moon derived using Kaguya topography. Icarus 208, 558–564.

Bussey, D.B., Sorensen, S.A., Spudis, P.D., 2009. Illumination and temperature modelling of the lunar polar regions. LPSC, p. 2027.

Bussey, D.B.J., Lucey, P.G., Steutel, D., Robinson, M.S., Spudis, P.D., Edwards, K.D., 2003. Permanent shadow in simple craters near the lunar poles. Geophys. Res. Lett. 30, 1278.

Chen, K.L., Tsang, K.T., Bruce, K., Zheng, Y.C., 2010. Lunar regolith thermal behavior revealed by Chang'E-1 microwave brightness temperature data. Earth Planet. Sci. Lett. 295, 287–291.

Chen, Y.L., Li, S.M., Liu, D.Y., 2009. Analysis of slope and aspect based on regular grid DEM. Geomat. Spatial Inf. Technol. 32 (5), 36–39.

Heiken, G., Vaniman, D., French, B.M., 1991. Lunar Source Book: A User's Guide to the Moon. Cambridge University Press, Cambridge.

Jaeger, J.C., 1953. The surface temperature of the Moon. Aust. J. Phys. 6, 10–21.

Jiang, J.S., Wang, Z.Z., Li, Y., 2008. Study on theory and application of CE-1 microwave sounding lunar surface. Eng. Sci. 10, 16–22.

Jones, W.P., Watkins, J.R., Calvert, T.A., 1975. Temperatures and thermophysical properties of the lunar outermost layer. The Moon 13, 475–494.

Keihm, S.J., Langseth, M.G., 1975. Lunar microwave brightness temperature observations reevaluated in the light of Apollo program findings. Icarus 24, 211–230.

Krotikov, V.D., Troitsky, V.S., 1964. Radio emission and nature of the Moon. Sov. Phys. Usp. 6, 841–871.

Li, C.L., Ren, X., Liu, J.J., et al., 2010a. Laser altimetry data of Chang'E-1 and the global lunar DEM model. Sci. China Ser. D 53 (11), 1582–1593.

Li, X.Y., Wang, S.J., Zheng, Y.C., Cheng, A.Y., 2008. Estimation of solar illumination on the Moon: a theoretical model. Planet. Space Sci. 56, 947–950.

Li, X.Y., Wang, S.J., Cheng, A.Y., 2007. A review of lunar-surface temperature model. Adv. Earth Sci. 22 (5), 480–485.

Li, Y., Wang, Z.Z., Jiang, J.S., 2010b. Simulations on the influence of lunar surface temperature profiles on CE-1 lunar microwave sounder brightness temperature. Sci. China Ser. D 53, 1379–1391.

Logan, L.M., Hunt, G.R., Balsamo, S.R., Salisbury, J.W., 1972. Midinfrared emission spectra of Apollo 14 and 15 soils and remote compositional mapping of the Moon. Proc. 3rd Lunar Sci. Conf. 3, 3069–3076.

Mazarico, E., Neumann, G.A., Smith, D.E., Zuber, M.T., Torrence, M.H., 2011. Illumination conditions of the lunar polar regions using LOLA topography. Icarus 211, 1066–1081.

Meng, Z.G., Chen, S.B., Du, X.J., Cui, T.F., 2010. Effective reflectivity of the lunar surface based on the laser altimeter data from the Chang'E-1 orbiter. J. Jilin Univ.: Earth Sci. Ed. 40 (3), 721–725.

Naugol'naya, M.N., Soboleva, N.S., 2001. A study of the lunar soil in regions with temperature anomalies. Sol. Syst. Res. 35, 35–45.

Neal, C.R., 2009. The Moon 35 years after Apollo: what's left to learn. Chem. Erde 69, 3–43.

Neukum, G., Jaumann, R., Hoffmann, H., Oberst, J., Wagner, R., Regner, P., Rebhan, H., Hiesinger, H., Dummel, A., 1991. Earth-based multispectral observations of the Moon. LPSC, p. 971.

Noda, H., Araki, H., Goossens, S., Ishihara, Y., Matsumoto, K., Tazawa, S., Kawano, N., Sasaki, S., 2008. Illumination conditions at the lunar polar regions by Kaguya (SELENE) laser altimeter. Geophys. Res. Lett. 35, L24203.

Paige, D.A., Matthew, A.S., Zhang, J.A., et al., 2010. Diviner lunar radiometer observations of cold traps in the Moon's south polar region. Science 330, 479–482. http://dx.doi.org/10.1126/science.1187726.

Ping, J.S., Huang, Q., Yan, J.G., Cao, J.F., Tang, G.S., Shu, R., 2009. Lunar topographic model CLTM-s01 from Chang'E-1 laser altimeter. Sci. China, Ser. G 52 (7), 1105–1114.

Racca, G.D., 1995. Moon surface thermal characteristics for Moon orbiting spacecraft thermal analysis. Planet. Space Sci. 43, 835–842.

Schloerb, F.P., Muhleman, D.O., Berge, G.L., 1976. Lunar heat flow and regolith structure inferred from interferometric observations at a wavelength of 49.3 cm. Icarus 29, 329–341.

Smith, R.E., West, G.S., 1983. Space and planetary environment criteria guidelines for use in space vehicle development, NASA TM 82478, MSFC, Alabama.

Tang, A.G., Liu, X.J., Yan, G.N., 2005. Principle and Application of the Digital Elevation Model and Geological Analysis. Science Press, Beijing.

Ulaby, F.T., Moore, R.K., Fung, A., 1981. Microwave Remote Sensing: Active and Passive. Addison-Wesley Publishing Company, Massachusetts.

Vasavada, A.R., Paige, D.A., Wood, S.E., 1999. Near-surface temperature on Mercury and the Moon and the stability of polar ice deposits. Icarus 141, 179–193.

Wang, Z.Z., Li, Y., Jiang, J.S., Li, D.H., 2010. Lunar surface dielectric constant, regolith thickness and helium-3 abundance distributions retrieved from microwave brightness temperatures of CE-1 lunar microwave sounder. Sci. China Ser. D 53 (9), 1365–1378.

Wesselink, A.J., 1948. Heat conductivity and nature of the lunar surface material. Bull. Astron. Inst. Neth. 10, 351–363.

Zhou, Q.M., Liu, X.J., 2006. Digital Terrain Analysis. Science Press, Beijing.